

Novae heat their food: mass transfer by irradiation

Sivan Ginzburg¹^{★†} and Eliot Quataert²

¹*Department of Astronomy and Theoretical Astrophysics Center, University of California, Berkeley, CA 94720, USA*

²*Department of Astrophysical Sciences, Princeton University, Princeton, NJ 08544, USA*

Accepted XXX. Received YYY; in original form ZZZ

ABSTRACT

A nova eruption irradiates and heats the donor star in a cataclysmic variable to high temperatures T_{irr} , causing its outer layers to expand and overflow the Roche lobe. We calculate the donor’s heating and expansion both analytically and numerically and find that irradiation drives enhanced mass transfer from the donor at a rate $\dot{m} \propto T_{\text{irr}}^{5/3}$, which reaches $\dot{m} \sim 10^{-6} \text{ M}_{\odot} \text{ yr}^{-1}$ at the peak of the eruption — about a thousand times faster than during quiescence. As the nova subsides and the white dwarf cools down, \dot{m} drops to lower values. We find that under certain circumstances, the decline halts and the mass transfer persists at a self-sustaining rate of $\dot{m} \sim 10^{-7} \text{ M}_{\odot} \text{ yr}^{-1}$ for up to $\sim 10^3$ yr after the eruption. At this rate, irradiation by the white dwarf’s accretion luminosity is sufficient to drive the mass transfer on its own. The self-sustaining rate is close to the white dwarf’s stable burning limit, such that this bootstrapping mechanism can simultaneously explain two classes of puzzling binary systems: recurrent novae with orbital periods ≈ 2 h (T Pyxidis and IM Normae) and long-lived supersoft X-ray sources with periods ≈ 4 h (RX J0537.7–7034 and 1E 0035.4–7230). Whether or not a system reaches the self-sustaining state is sensitive to the donor’s chromosphere structure, as well as to the orbital period change during nova eruptions.

Key words: novae, cataclysmic variables – binaries: close – stars: individual: T Pyxidis – stars: individual: IM Normae

1 INTRODUCTION

Cataclysmic variables (CVs) are binary systems in which a main sequence donor star fills its Roche lobe and transfers mass to a white dwarf. As hydrogen accumulates on the white dwarf’s surface, the density and temperature at the base of the accreted layer rise. At some point, a critical mass is reached, and the accumulated layer explodes in a thermonuclear runaway — a nova. The binary system survives the explosion, mass accumulates once again on top of the white dwarf, and the nova recurs on a time-scale that depends on the accretion rate and on the white dwarf’s mass (e.g. [Gallagher & Starrfield 1978](#); [Shara 1989](#); [Prialnik & Kovetz 1995](#); [Townsend & Bildsten 2004](#); [Yaron et al. 2005](#); [Wolf et al. 2013](#); [Chomiuk et al. 2020](#)).

During and immediately after a nova eruption, the white dwarf’s luminosity is close to the Eddington limit ([Prialnik 1986](#); [Gehrz et al. 1998](#)). The companion is irradiated and heated to a surface temperature that is an order of magnitude hotter than its pre-eruption (main sequence) effective temperature. [Kovetz et al. \(1988\)](#) studied the response of the companion to such irradiation and calculated the heat penetration into its atmosphere. As the heated layers expand, the donor overflows its Roche lobe more than in quiescence, and the mass transfer rate increases by orders of magnitude. Recently, [Hillman et al. \(2020\)](#) demonstrated that this irradiation-driven enhanced mass transfer may dominate the long term evolution of CVs over multiple nova cycles.

Here, we revisit the heating of the donor star by the hot white dwarf during and after a nova eruption using a combination of analytical

arguments and experiments with the MESA stellar evolution code ([Paxton et al. 2011, 2013](#)). We calculate the enhanced mass transfer rate following a nova and improve upon [Kovetz et al. \(1988\)](#) and [Hillman et al. \(2020\)](#) by refining their power-law scaling for how this rate depends on the irradiation temperature and on the donor’s mass. More importantly, we revise upwards the normalization of the mass transfer rate.

Finally, we discuss the decline of the mass transfer rate back to quiescence as the white dwarf cools down after a nova. We find that under certain conditions, the decline halts and the mass transfer becomes self-sustaining: the white dwarf’s accretion luminosity is enough to drive the accreted mass through the irradiated companion’s Roche lobe. This ‘bootstrapping’ state may explain the high quiescent accretion rates ($\sim 10^{-7} \text{ M}_{\odot} \text{ yr}^{-1}$) recently observed for the recurrent novae T Pyxidis (T Pyx) and IM Normae (IM Nor) ([Patterson et al. 2017, 2020](#); [Godon et al. 2018](#)). If the self-sustaining rate is sufficiently high, the white dwarf can burn accreted hydrogen stably ([Nomoto et al. 2007](#); [Shen & Bildsten 2007](#); [Wolf et al. 2013](#)), potentially explaining long-lived supersoft X-ray sources with short orbital periods like RX J0537.7–7034 and 1E 0035.4–7230 as well ([Kahabka & van den Heuvel 1997](#); [King et al. 2001](#)).

The remainder of this paper is organized as follows. In Section 2 we analyse the Roche-lobe filling during quiescence, and in Section 3 we study the response of the companion to a nova outburst. Our main results — the enhanced mass transfer rates — are presented in Section 4, where we also compare to previous works (Section 4.1) and discuss the self-sustaining bootstrapping state (Section 4.2). We summarize our findings in Section 5.

[★] E-mail: ginzburg@berkeley.edu

[†] 51 Pegasi b Fellow.

2 QUIESCENCE

Between nova eruptions, the binary loses angular momentum by magnetic braking and gravitational waves on a \sim Gyr time-scale, and the companion (donor) star is driven towards stable Roche-lobe overflow (e.g. Rappaport et al. 1983; Spruit & Ritter 1983; Knigge et al. 2011). The companion, with a mass m and a radius r , overflows its Roche lobe r_L by $\Delta r \equiv r - r_L \ll r$ such that the mass transfer rate \dot{m} through the L1 Lagrange point follows the angular momentum loss rate (up to an order-unity factor; see Rappaport et al. 1982) $\dot{m} \sim 10^{-10} - 10^{-9} M_\odot \text{ yr}^{-1}$.¹ Note that the photosphere can be either interior or exterior to the Roche lobe; a negative Δr is discussed towards the end of this section.

We estimate the overfilling length Δr using the standard calculation, in which the overflowing companion's surface is modelled as a sphere, truncated at a depth Δr by the Roche potential (e.g. Paczyński & Sienkiewicz 1972; Savonije 1978; Ritter 1988; Kolb & Ritter 1990; Marsh et al. 2004; Linial & Sari 2017). The mass flow rate through the L1 nozzle is given by (we omit uncertain order-unity coefficients)

$$\dot{m} \sim \rho c_s r \Delta r, \quad (1)$$

where ρ and c_s are the density and sound speed at depth Δr inside the companion's atmosphere, respectively (the flow reaches sonic velocities at L1; Lubow & Shu 1975), and where the nozzle's cross section is $r^2 - (r - \Delta r)^2 \sim r \Delta r$. We normalize \dot{m} using

$$\dot{m}_{\text{ph}} \equiv \dot{m}(\Delta r \approx h) \sim \left(\frac{k T_{\text{eff}}}{\mu} \right)^{3/2} \frac{r^3}{G m} \rho_{\text{ph}}, \quad (2)$$

which is the mass loss rate of companions that overflow their Roche lobe by a photospheric scale height $h = k r^2 T_{\text{eff}} / (G m \mu)$, where G , k , and μ denote the gravitational constant, Boltzmann's constant, and the molecular weight, respectively; T_{eff} is the donor's effective temperature. We estimate the photospheric density ρ_{ph} using the condition

$$\kappa \rho_{\text{ph}} h \sim 1, \quad (3)$$

where the opacity $\kappa \propto \rho_{\text{ph}}^{1/2} T_{\text{eff}}^9$ is dominated by H^- for typical M dwarf companions with $T_{\text{eff}} \sim 3 \times 10^3 \text{ K}$ (e.g. Hansen et al. 2004). We substitute ρ_{ph} in equation (2) and find (see also Ritter 1988)

$$\dot{m}_{\text{ph}} \propto r^{5/3} m^{-1/3} T_{\text{eff}}^{-31/6} \sim 10^{-8} M_\odot \text{ yr}^{-1}. \quad (4)$$

We rewrite equation (1) as

$$\dot{m} \sim \dot{m}_{\text{ph}} \frac{\rho}{\rho_{\text{ph}}} \left(\frac{T}{T_{\text{eff}}} \right)^{1/2} \frac{\Delta r}{h}, \quad (5)$$

where T is the temperature at depth Δr .

Assuming a polytrope with an index n , the structure of the star (for $h < \Delta r \ll r$) is given by

$$\frac{\rho}{\rho_{\text{ph}}} \sim \left(\frac{T}{T_{\text{eff}}} \right)^n \sim \left(\frac{\Delta r}{h} \right)^n. \quad (6)$$

The mass loss rate in this case is

$$\dot{m} \sim \dot{m}_{\text{ph}} \left(\frac{\Delta r}{h} \right)^{n+3/2}. \quad (7)$$

Equations (6) and (7) break down when the mass loss is slow enough

such that Δr falls inside the star's photosphere, which has a scale height $h/r \sim T_{\text{eff}}/T_c$, where $T_c \sim G m \mu / (k r) \sim 10^7 \text{ K}$ is the star's central temperature. For lower \dot{m} , the photosphere *underfills* the Roche lobe by several scale heights (i.e. $\Delta r < 0$), the profile is isothermal with $T \approx T_{\text{eff}}$, and the density ρ falls off exponentially from the photosphere towards L1 (Ritter 1988). We extend equation (7) to the photospheric case:

$$\frac{\dot{m}}{\dot{m}_{\text{ph}}} \sim \begin{cases} (\Delta r/h)^{n+3/2} & +\Delta r > h \\ \exp(\Delta r/h) & -\Delta r \gtrsim h. \end{cases} \quad (8)$$

We conclude that during quiescence — when $\dot{m} \ll \dot{m}_{\text{ph}}$ — the companion star's photosphere underfills its Roche lobe by several $h \sim 3 \times 10^{-4} r$ (i.e. the Roche lobe is offset by $\Delta r_L \equiv -\Delta r \sim 10^{-3} r$). The exact value of Δr_L depends on the star's structure exterior to the photosphere, potentially reaching the chromosphere, where the star's atmosphere heats up beyond T_{eff} .

3 NOVA ERUPTION

3.1 Heat penetration

When a nova erupts, it irradiates the companion star and sets an outer boundary temperature $T_{\text{irr}} > T_{\text{eff}}$. This hot layer gradually penetrates deeper (in a Lagrangian sense) by diffusion, heating a progressively larger mass to a temperature $\approx T_{\text{irr}}$ (Kovetz et al. 1988). The time it takes to heat a layer with a mass $\Delta m \ll m$ by diffusion to a temperature $T \gtrsim 10^4 \text{ K}$ is

$$t \sim \frac{\Delta m k T / \mu}{4 \pi r^2 \sigma T_{\text{irr}}^4 / \tau} \sim \frac{\kappa k \Sigma^2 T}{\mu \sigma T_{\text{irr}}^4} \propto \frac{m \Sigma^3}{r^2 T_{\text{irr}}^4 T^{7/2}}, \quad (9)$$

where τ is the layer's optical depth and σ denotes the Stefan–Boltzmann constant. In the second similarity in equation (9) we used $\tau \sim \kappa \Sigma$, where $\Sigma \equiv \Delta m / (4 \pi r^2)$ is the mass column density. In the final proportionality, we assumed Kramers' opacity $\kappa \propto \rho T^{-7/2}$ (e.g. Hansen et al. 2004; Kippenhahn et al. 2012), and used $\Sigma \sim \rho h$, where the heated layer expands by a scale height $h = k r^2 T / (G m \mu)$. Equation (9) indicates that the heating time to T_{irr} is actually dominated by the time spent at lower temperatures $T < T_{\text{irr}}$, such that the penetration of the heat with time scales as

$$\Delta m_{\text{heat}}(t) = 4 \pi r^2 \Sigma(t) \propto r^{8/3} m^{-1/3} T_{\text{irr}}^{4/3} t^{1/3}. \quad (10)$$

3.1.1 Numerical computation

In Fig. 1 we present numerical calculations of the heat penetration into a $0.25 M_\odot$ companion, performed using the stellar evolution code MESA (Paxton et al. 2011, 2013, 2015, 2018, 2019). We implement the irradiation using the $F_\star - \Sigma_\star$ method (Paxton et al. 2013): $F_\star = 4 \sigma T_{\text{irr}}^4$ is the incoming flux, which we parametrize using the induced effective temperature T_{irr} (assuming efficient redistribution between the two hemispheres), and $\Sigma_\star = 3 \text{ g cm}^{-2}$ is the mass column density for electron scattering, which sets an upper limit on the irradiation depth. As seen in Fig. 1, the heat penetrates into $\Sigma > \Sigma_\star$ in less than 0.1 h, so our results are not sensitive to the exact value of Σ_\star . For numerical convenience, we linearly increase the flux from zero to F_\star over a rise time of $t = 100 \text{ s}$, which is much shorter than any relevant time-scale in the problem. Fig. 1 agrees well with the analytical scaling found in equation (10).

¹ Throughout the paper, \dot{m} is to be understood as $|\dot{m}|$, where we omit the absolute value sign for brevity.

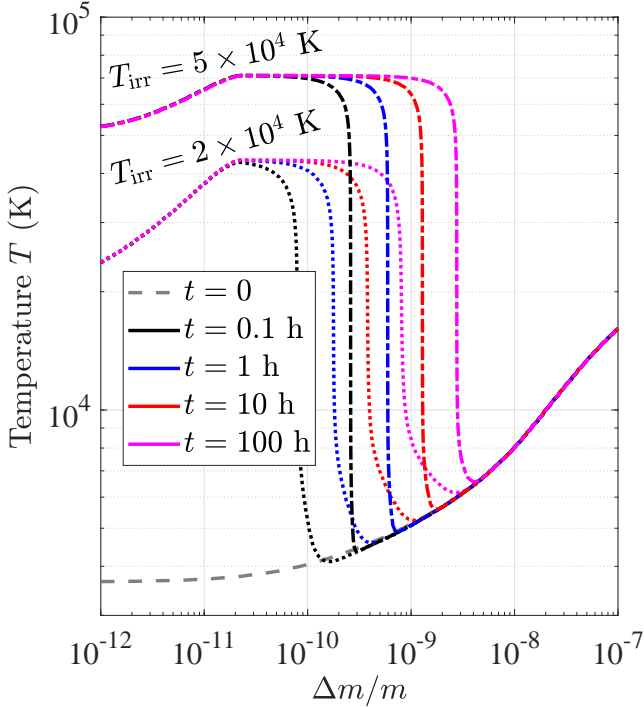


Figure 1. Heat penetration into an $m = 0.25 M_{\odot}$ companion, calculated using MESA for two nova irradiation temperatures $T_{\text{irr}} = 2 \times 10^4$ K (dotted lines) and $T_{\text{irr}} = 5 \times 10^4$ K (dot-dashed lines). The heating begins at $t = 0$ (dashed grey line) and penetrates progressively deeper into the companion $\Delta m_{\text{heat}} \propto t^{1/3}$.

3.2 Boosted Roche-lobe overflow

During a nova eruption, the heated outer layers of the companion expand such that it overflows its Roche lobe more than in quiescence — significantly amplifying the mass transfer through L1. Unlike quiescence, a nova outburst is too short for magnetic braking or gravitational waves to adjust the orbit and the size of the Roche lobe — m/\dot{m} is now decoupled from these angular momentum loss mechanisms (we discuss faster orbital change below).

We calculate the mass transfer rate \dot{m} similarly to Section 2:

$$\dot{m} \equiv \dot{m}_{\text{loss}} \sim \rho c_s r \Delta r \sim \rho r^2 h \frac{c_s}{r} \sim \frac{c_s}{r} \Delta m_{\text{heat}} \sim \frac{c_s t}{r} \dot{m}_{\text{heat}}, \quad (11)$$

where $\Delta r \sim h(T_{\text{irr}}) = k r^2 T_{\text{irr}} / (G m \mu)$ is the inflation beyond the Roche lobe. Since in quiescence $\Delta r \sim -h(T_{\text{eff}})$, and since the heated layers expand by a larger scale height $h(T_{\text{irr}} > T_{\text{eff}})$ once the nova erupts, we approximately identify the Roche lobe with the companion's radius before eruption, i.e. $r(t = 0)$; see details below. The density ρ at the bottom of the heated (and inflated) zone is given by the mass that the heat has penetrated by time t , as calculated in Section 3.1: $\rho r^2 h \sim \Delta m_{\text{heat}}(t)$. The speed of sound is $c_s \sim (k T_{\text{irr}} / \mu)^{1/2}$.

Equation (11) is applicable only for times $t \leq t_{\text{max}} = r/c_s$. The outer layers of the companion, which are being heated by the irradiation, are the same layers that are being lost through Roche-lobe overflow. As the heated mass is removed, new cool layers are exposed to the heating, requiring $\dot{m}_{\text{loss}} \leq \dot{m}_{\text{heat}} \equiv d\Delta m_{\text{heat}}(t)/dt$ for a consistent solution (Harpaz & Rappaport 1991). In other words, up to a time t_{max} , only a fraction of the heated mass has been removed ($\Delta m_{\text{loss}} \propto t^{4/3} < \Delta m_{\text{heat}} \propto t^{1/3}$). At later times $t > t_{\text{max}}$, the heating and mass loss reach a steady state in which a layer $\Delta m_{\text{heat}}(t_{\text{max}})$ is being both heated and lost on a time-scale t_{max} . We conclude that

the mass transfer rate \dot{m} saturates at

$$\dot{m}_{\text{loss}} \sim \dot{m}_{\text{heat}} \sim \frac{\Delta m_{\text{heat}}(t_{\text{max}})}{t_{\text{max}}} \propto r^2 m^{-1/3} T_{\text{irr}}^{5/3} \propto m^{1.3} T_{\text{irr}}^{5/3} \quad (12)$$

with $\Delta m_{\text{heat}}(t)$ calculated in equation (10). We note that while our one-dimensional hydrostatic MESA calculation of $\Delta m_{\text{heat}}(t)$ is inadequate for time-scales much shorter than the sound crossing time r/c_s , it should be accurate to within order-unity corrections for $t = t_{\text{max}} = r/c_s$ itself. For the final proportionality in equation (12) we assumed $r \propto m^{0.8}$ (e.g. Kippenhahn et al. 2012).

In Fig. 2 we plot profiles of irradiated companions at the saturation time $t = t_{\text{max}}(T_{\text{irr}})$ — these depict the steady-state structure of the companion, from which the mass transfer rate \dot{m} is determined. The figure demonstrates that the companion star is inflated by $\Delta r/r \sim h/r \sim T_{\text{irr}}/T_c \sim 10^{-3} - 10^{-2}$. The bottom panel shows that the density of the inflated region ρ is a weak function of T_{irr} : a higher T_{irr} heats a larger mass Δm_{heat} , but this mass is spread over a larger $h \propto T_{\text{irr}}$:

$$\rho \sim \frac{\Delta m_{\text{heat}}}{4\pi r^2 h} \propto \frac{T_{\text{irr}}^{4/3} t_{\text{max}}^{1/3}}{T_{\text{irr}}} \propto T_{\text{irr}}^{1/6}, \quad (13)$$

where we substituted Δm_{heat} from equation (10) and $t_{\text{max}} = r/c_s$.

The temperature and density profiles in Fig. 2 are approximately flat in the $-10^{-4} \leq \Delta r/r \leq h/r \sim 10^{-3} - 10^{-2}$ region (the extent of the flat region with $\Delta r < 0$ is determined by heating and expansion at the precursor just below the heating front), where Δr is measured relative to the radius of a non-irradiated companion, i.e. $r(t = 0)$. We may therefore approximately identify $r_L = r(0)$, when the Roche lobe actually exceeds the photosphere by $\Delta r_L/r \sim 10^{-3}$ (Section 2); this approximation holds for the high $T_{\text{irr}} \approx 5 \times 10^4$ K at the peak of a nova eruption, but breaks down as the white dwarf cools. In Section 4.2.1 we repeat the calculation with $\Delta r_L/r \sim 10^{-3}$, which is relevant for lower T_{irr} , when the eruption subsides.

Mass ejection from the white dwarf during the nova can expand the orbit of the binary and therefore the companion's Roche lobe by a fraction $\sim 10^{-5}$ (of order the lost mass fraction; see Shara et al. 1986). While this small effect can be neglected in the calculation above, some (many decades old) novae have been recently claimed to shrink the binary orbit (and consequently the Roche lobe) by as much as $\sim 10^{-4} - 10^{-3}$ (Salazar et al. 2017; Schaefer 2020), which might be enough to modify our \dot{m} estimate. Since we lack a clear picture of how the binary orbit changes during the nova (see Chomiuk et al. 2020, for a recent review) we ignore this possibility and determine \dot{m} using $r_L(t = 0)$. While we assume that changes to r_L during an eruption can be neglected when calculating a single nova cycle, these changes can accumulate over multiple cycles and affect the long term evolution of CVs; we briefly discuss this in Section 4.2.2.

4 MASS TRANSFER RATES

In Fig. 3 we calculate the mass transfer rates \dot{m} from MESA profiles at $t = t_{\text{max}} = r/c_s$ using two methods:

(i) *Direct*: $\dot{m} = \rho c_s r \Delta r$, with ρ and c_s evaluated at $r(t = 0)$ and with $\Delta r = r(t_{\text{max}}) - r(0)$. That is, we identify the Roche lobe with the companion's quiescent radius (see Fig. 2).

(ii) *Heated layer*: $\dot{m} = \Delta m_{\text{heat}}/t_{\text{max}}$, where Δm_{heat} is the mass that is heated above $T_{\text{irr}}/2$. The heating front is very sharp, such that we are not sensitive to the exact threshold; see Fig. 1.

In light of the discussion in Section 3.2, the two methods should be equivalent up to an order-unity factor. This is confirmed by Fig.

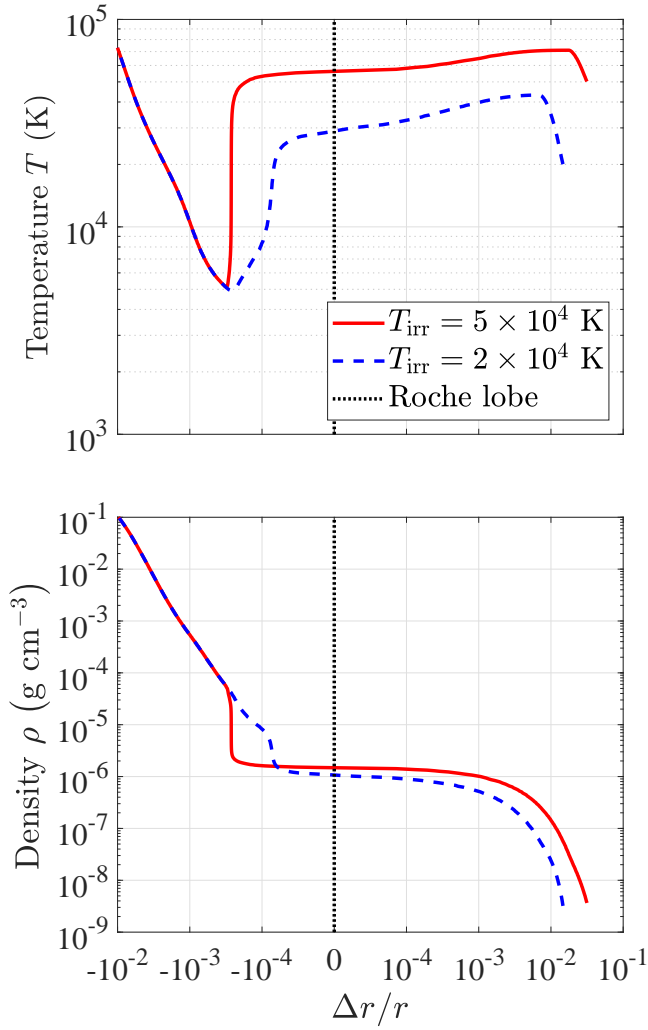


Figure 2. Temperature (top panel) and density (bottom panel) profiles of irradiated $0.25 M_{\odot}$ companions at the saturation time $t = t_{\text{max}} = r/c_s \propto T_{\text{irr}}^{-1/2}$ for irradiation temperatures $T_{\text{irr}} = 2 \times 10^4$ K (dashed blue lines, $t = 3.8$ h) and $T_{\text{irr}} = 5 \times 10^4$ K (solid red lines, $t = 2.4$ h). The radial coordinate Δr is measured relative to the Roche lobe r_L (dotted black lines), which we approximately identify here with the companion’s radius at $t = 0$ (this is a slight underestimate because in quiescence $\Delta r_L/r \sim 10^{-3}$; we refine the calculation in Section 4.2.1). The horizontal axis is logarithmic on both sides of the Roche lobe, with the $|\Delta r|/r < 10^{-5}$ region excised.

3, which also agrees with the analytical scaling found in equation (12): $\dot{m} \propto m^{1.3} T^{5/3}$. Below $T_{\text{irr}} \lesssim 2 \times 10^4$ K many of our model’s assumptions break down. Specifically, the opacity can no longer be approximated by Kramers’ law, and T_{irr} becomes comparable to the donor’s quiescent temperature, smearing the heating front. The heating at the precursor below the front (Fig. 1) leads to its expansion, such that r_L no longer falls inside the region with flat T and ρ (Fig. 2). Both our numerical methods and the analytical solution lose accuracy at these low irradiation temperatures. As we show below, we are interested mainly in $T_{\text{irr}} \gtrsim 2 \times 10^4$ K anyway; we provide the direct solution for $T_{\text{irr}} < 2 \times 10^4$ K in Fig. 3 only as a rough approximation.

Following a short thermonuclear runaway at the onset of a nova eruption, the white dwarf’s luminosity reaches $\sim 10^{38} \text{ erg s}^{-1}$ — similar to the Eddington luminosity — equivalent to $T_{\text{irr}} \approx 5 \times$

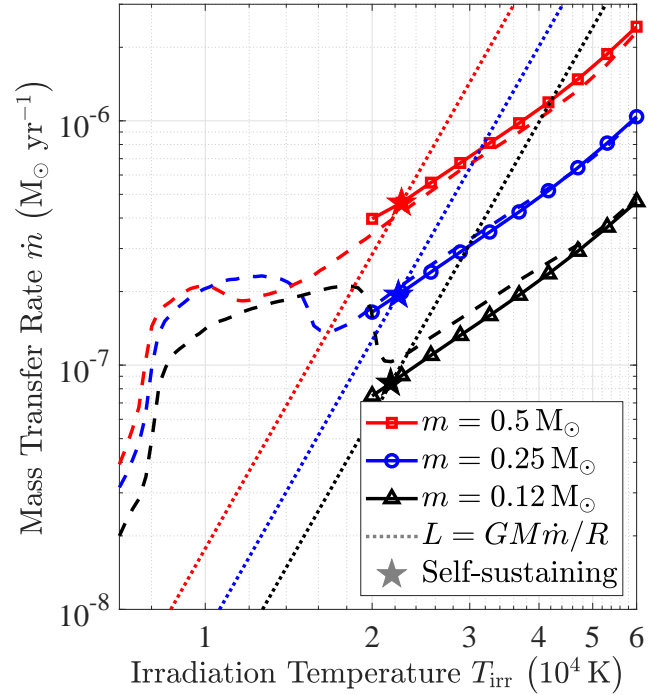


Figure 3. Mass transfer rates calculated from MESA using two methods: directly, $\dot{m} = \rho c_s r \Delta r$, using ρ , c_s , and Δr at the Roche lobe (dashed lines), and indirectly, using the heating rate $\dot{m} = \Delta m_{\text{heat}}(t_{\text{max}})/t_{\text{max}}$ (solid lines with markers). The two methods are consistent for $T_{\text{irr}} \gtrsim 2 \times 10^4$ K and agree with our analytical scaling $\dot{m} \propto m^{1.3} T_{\text{irr}}^{5/3}$ (equation 12). $T_{\text{irr}} = 5.4 \times 10^4$ K corresponds to a nova luminosity of $L = 16\pi a (M, m)^2 \sigma T_{\text{irr}}^4 = 10^{38} \text{ erg s}^{-1}$ for an $m = 0.25 M_{\odot}$ companion orbiting an $M = 1 M_{\odot}$ white dwarf (using Eggleton 1983 to calculate the binary separation a). The dotted lines mark \dot{m} that is required to sustain an accretion luminosity $L = GM\dot{m}/R = 16\pi a (m)^2 \sigma T_{\text{irr}}^4$ from a solar mass white dwarf. The mass transfer becomes self-sustaining at the intersection of the lines, marked with a star ($\equiv T_{\text{irr}}^0 \approx 2 \times 10^4$ K, with $\dot{m} \sim 10^{-7} M_{\odot} \text{ yr}^{-1}$).

10^4 K on the companion’s surface (Prialnik 1986; Gehrz et al. 1998; Chomiuk et al. 2020). According to Fig. 3, the mass transfer rate reaches $\sim 10^{-6} M_{\odot} \text{ yr}^{-1}$ — about a thousand times the quiescent value set by gravitational waves and magnetic braking (Patterson 1984). The white dwarf then cools down, and over a time-scale of roughly a year its luminosity drops by two orders of magnitude, such that $T_{\text{irr}} \approx 2 \times 10^4$ K (Prialnik 1986; Hillman et al. 2014). It is clear from Section 3.2 that \dot{m} adjusts to changes in T_{irr} on a time-scale of r/c_s , which is measured in hours — practically instantaneously compared to the decline of T_{irr} .

4.1 Comparison with previous calculations

Kovetz et al. (1988) conducted similar calculations of the response of a red dwarf companion to a nova eruption. More recently, Hillman et al. (2020) evolved CVs for several gigayears and through numerous nova eruptions, incorporating the effects of nova irradiation as calculated by Kovetz et al. (1988). While the penetration of heat into the companion’s atmosphere is calculated similarly here and in Kovetz et al. (1988), the inference of the mass transfer rate \dot{m} is conceptually different.

Kovetz et al. (1988) assumed that the density ρ at L1 remains similar to the photospheric density of the quiescent star ρ_{ph} , up to an exponential factor of order unity (because $\Delta r \sim h$). The resulting

mass transfer rate in their case is $\dot{m} \sim \rho_{\text{ph}} r c_s(T_{\text{irr}}) h(T_{\text{irr}}) \propto T_{\text{irr}}^{3/2}$. We, on the other hand, find $\rho \propto T_{\text{irr}}^{1/6}$ by consistently calculating the mass and expansion of the heated zone (equation 13) — yielding $\dot{m} \propto \rho r c_s h \propto T_{\text{irr}}^{5/3}$. In addition, equation (12) indicates that for the same T_{irr} , $\dot{m} \propto m^{1.3}$, much steeper than the mass dependence found by Kovetz et al. (1988, their table 3).

More important than correcting these power laws (the dependence on the temperature hardly changes) is normalizing them. Kovetz et al. (1988) arbitrarily calibrate $\dot{m} = 10^{-9} M_{\odot} \text{ yr}^{-1}$ for a $0.5 M_{\odot}$ companion 100 yr after an eruption. Hillman et al. (2020) suggest that the mass transfer rate is enhanced by a factor of $(T_{\text{irr}}/T_{\text{eff}})^{3/2} \sim 10^2$ relative to quiescence. In our model, on the other hand, the quiescent \dot{m} is unrelated to T_{eff} : as explained in Section 2, the Roche-lobe overflowing length $\Delta r(\dot{m})$ adjusts to accommodate the mass transfer rate, which is set by magnetic braking and gravitational waves. Consequently, there is no ‘enhancement factor’: \dot{m} during and immediately after a nova eruption is a function of T_{irr} and m alone, regardless of the quiescent rate — the normalization is given in Fig. 3. The bottom line is that we find mass transfer rates that are more than an order of magnitude higher than Kovetz et al. (1988) and Hillman et al. (2020).

4.2 Bootstrapping (self-sustaining accretion)

Fig. 3 shows that as the white dwarf cools down, and \dot{m} decreases, the mass transfer onto the white dwarf becomes self-sustaining. At the intersection of the solid and dotted lines, \dot{m} is just enough to lift itself out through L1 using the accretion luminosity $L = GM\dot{m}/R$ (M and R are the white dwarf’s mass and radius, respectively). We find that the self-sustaining rate is $\dot{m} \sim 10^{-7} M_{\odot} \text{ yr}^{-1}$ (equivalently $L \sim 10^{36} \text{ erg s}^{-1}$), providing a possible explanation for the puzzling high accretion rates of the recurrent novae T Pyx and IM Nor during quiescence (Patterson et al. 2017, 2020; Godon et al. 2018). Knigge et al. (2000) proposed a different self-sustaining mechanism for T Pyx: an irradiation-driven wind carries away angular momentum from the binary, driving the companion to overflow its Roche lobe. Knigge et al. (2000) rely on stable nuclear burning to power the evaporation (see Section 4.2.3), whereas our mechanism can explain T Pyx with the accretion luminosity alone (which is weaker by a factor of ≈ 30). Moreover, our mechanism remains valid even if the binary conserves its total mass and angular momentum.

4.2.1 Roche-lobe offset

This high quiescent accretion rate might not follow all novae, as also suggested observationally (Patterson et al. 2017, 2020), because it depends critically on the size of the donor’s Roche lobe. In Sections 3 and 4 we have so far assumed that the companion’s Roche lobe r_L coincides with its un-inflated radius $r(t=0)$. In Section 2, however, we found that angular momentum loss by magnetic braking and gravitational waves dictates an offset of $\Delta r_L \equiv r_L - r(0) \sim 10^{-3} r$. We repeat the calculation in Section 3.2 with $\Delta r_L > 0$ and find that

$$\dot{m} \sim \rho c_s r (h - \Delta r_L) \sim \Delta m_{\text{heat}}(t) \frac{c_s}{r} \left(1 - \frac{\Delta r_L}{h} \right). \quad (14)$$

Equation (14) saturates at $t_{\text{max}} = (r/c_s)(1 - \Delta r_L/h)^{-1} > r/c_s$ and the mass transfer rate scales as

$$\dot{m} \sim \frac{\Delta m_{\text{heat}}(t_{\text{max}})}{t_{\text{max}}} \propto T_{\text{irr}}^{5/3} \left[1 - \frac{\Delta r_L}{h(T_{\text{irr}})} \right]^{2/3}. \quad (15)$$

At the peak of a nova eruption, the offset Δr_L hardly changes \dot{m} because $\Delta r_L/h(T_{\text{irr}}) \sim 0.1$. During the cooler self-sustaining accretion

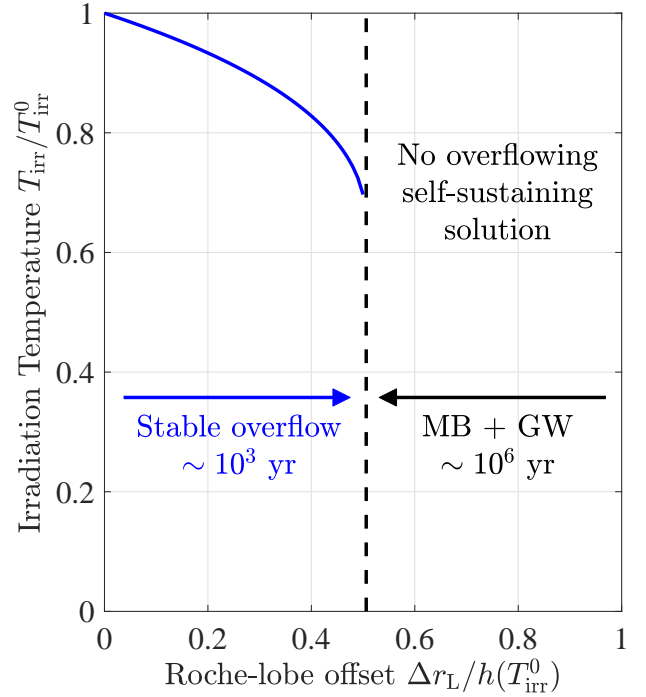


Figure 4. The self-sustaining (bootstrapping) irradiation temperature $T_{\text{irr}} \propto \dot{m}^{1/4}$ as a function of $\Delta r_L \equiv r_L - r(0)$, the difference between the donor’s Roche lobe r_L and its non-irradiated radius $r(0)$. $T_{\text{irr}}^0 \equiv T_{\text{irr}}(\Delta r_L = 0) \approx 2 \times 10^4 \text{ K}$ is calculated in Fig. 3, and $h(T_{\text{irr}}^0) \sim 10^{-3} r$ is the corresponding scale height. The curve is given by equation (16), which has no solution for $\Delta r_L/h(T_{\text{irr}}^0) > 0.51$, where the donor recedes within its Roche lobe and \dot{m} drops steeply. Stable Roche-lobe overflow increases Δr_L by the critical $\sim 10^{-3} r$ over $t \sim 10^3 \text{ yr}$, whereas angular momentum loss by magnetic braking (MB) and gravitational waves (GW) decreases Δr_L by a similar amount over $t \sim 10^6 \text{ yr}$ — bootstrapping with a quiescent $\dot{m} \sim 10^{-7} M_{\odot} \text{ yr}^{-1}$ is a short lived phase (though the exact long term evolution of Δr_L is uncertain; see Section 4.2.2).

phase that follows, on the other hand, h becomes comparable to Δr_L — significantly lowering \dot{m} and with it $h \propto T_{\text{irr}} \propto L^{1/4} \propto \dot{m}^{1/4}$. Using equation (15), the self-sustaining irradiation temperature $T_{\text{irr}}(\Delta r_L) \propto \dot{m}^{1/4}$ scales as $T_{\text{irr}} \propto (1 - \Delta r_L/h)^{2/7}$. Explicitly,

$$\frac{T_{\text{irr}}}{T_{\text{irr}}^0} = \left[1 - \frac{\Delta r_L}{h(T_{\text{irr}}^0)} \frac{T_{\text{irr}}^0}{T_{\text{irr}}} \right]^{2/7}, \quad (16)$$

where $T_{\text{irr}}^0 \approx 2 \times 10^4 \text{ K}$ is the solution for $\Delta r_L = 0$ (i.e. the star markers in Fig. 3) and $h(T_{\text{irr}}^0) \sim 10^{-3} r$ is the corresponding scale height. We solve equation (16) for different values of Δr_L in Fig. 4. As Δr_L increases, the self-sustaining $T_{\text{irr}} \propto \dot{m}^{1/4}$ gradually drops; there is no solution for $\Delta r_L/h(T_{\text{irr}}^0) > 0.51$ — the donor recedes within its Roche lobe and the mass transfer rate drops exponentially (see Section 2).

4.2.2 Long term evolution

Why do some novae remain locked in the self-sustaining state whereas others decline to lower quiescent accretion rates? The Roche-lobe’s size before and immediately after an eruption may hold the key. The exact value of Δr_L before the eruption depends on the donor’s density structure at several scale heights above the photosphere, as indicated by equation (8). At such heights, the profile might deviate

from our isothermal approximation due to heating by e.g. magnetic fields (Avrett & Loeser 2008), making it hard to establish in which of the two regimes of Fig. 4 Δr_L falls.

Even if the donor initially satisfies $\Delta r_L < 0.51h(T_{\text{irr}}^0) \sim 10^{-3}r$, the high self-sustaining accretion rate may not last indefinitely because the size of the Roche lobe changes over time. The mass transfer in CVs is stable — it increases Δr_L and drives the companion away from Roche-lobe overflow ($(1/r)d\Delta r_L/dt \sim \dot{m}/m$ (the orbit expands to conserve angular momentum; see Rappaport et al. 1982). At the self-sustaining mass transfer rate of $\dot{m} \sim 10^{-7} \text{ M}_{\odot} \text{ yr}^{-1}$, the critical offset of $\Delta r_L \sim 10^{-3}r$ is reached within $t \sim 10^3 \text{ yr}$, ending the bootstrapping phase. Loss of angular momentum by magnetic braking and gravitational waves pushes the companion back towards Roche-lobe overflow and decreases Δr_L , but this process unfolds on a longer time-scale: it takes $\sim \text{Gyr}$ to shrink the orbit by half, and hence $t \sim 10^6 \text{ yr}$ to decrease Δr_L by $10^{-3}r$. This asymmetry in time-scales may explain why T Pyx and IM Nor are the exception rather than the rule (most novae decline to much lower accretion rates by a similar time after eruption; see Patterson et al. 2017, 2020, but also the discussion of recurrence times below).

Multiple novae can erupt during both bootstrapping periods (when Δr_L is small such that the quiescent $\dot{m} \sim 10^{-7} \text{ M}_{\odot} \text{ yr}^{-1}$) and dormant times (when Δr_L is large such that $\dot{m} \sim 10^{-10} - 10^{-9} \text{ M}_{\odot} \text{ yr}^{-1}$, as set by magnetic braking and gravitational waves). The higher accretion rate during bootstrapping drives novae more frequently (Yaron et al. 2005; Wolf et al. 2013; Chomiuk et al. 2020), explaining the short recurrence times of T Pyx and IM Nor (10–100 yr). Dormant periods last $\sim 10^3$ times longer than bootstrapping, but the nova recurrence time is also longer by a similar factor, producing roughly the same total number of novae. T Pyx and IM Nor represent about a third of the novae in short-period CVs in the Patterson et al. (2020) sample (shorter than about 3 h; T Pyx should be counted twice because a high \dot{m} was measured after both the 1966 and 2011 eruptions, see Patterson et al. 2017); the ratio drops to about 10 per cent when longer period systems are included.

We note that orbital periods and therefore Δr_L jump during eruptions due to ejection of mass and angular momentum (see discussion in Section 3.2), which might induce or end a bootstrapping phase. The sign and magnitude of these jumps is uncertain (Chomiuk et al. 2020), complicating our analysis of the relative numbers of the two nova populations. As an extreme example, if each nova shrinks the orbit by an average fraction of $10^{-5} - 10^{-4}$, then eruptions during bootstrapping can counter the expansion of Δr_L over the 10–100 yr recurrence time between novae, when $m/\dot{m} \sim 10^6 \text{ yr}$. In this case, the bootstrapping phase may proceed all the way up to the donor’s destruction (as suggested by Patterson et al. 2017, 2020), which might be further accelerated by unstable mass transfer (triggered by the angular momentum loss in the novae; see Schreiber et al. 2016). While the 2011 T Pyx eruption actually *increased* its orbital period (Patterson et al. 2017) — expediting the end of bootstrapping — some novae might shrink the orbit enough to keep systems in the high \dot{m} state (see table S2 in Chomiuk et al. 2020).

It is important to stress that in our model some variation in either Δr_L during quiescence (e.g. due to variations from star to star in the upper atmosphere structure of M dwarf donors) or in the orbital period jumps during novae is required to explain why — at the same orbital period — some systems are trapped in a self-sustaining state while others are not. Absent such variation from system to system we would expect all systems of a given orbital period and white dwarf mass to eventually evolve towards one or the other of the two solution regimes in Fig. 4. One possibility is that eruptions during bootstrapping change the orbital period differently from ‘reg-

ular’ novae because of the higher \dot{m} before eruptions. The higher accretion rate raises the temperature of the accreted layer, implying a somewhat lower hydrogen ignition mass (fig. 8 in Wolf et al. 2013). When the nova erupts, the lighter expelled shell in this case is expected to exert less friction on the binary — removing less angular momentum (Livio et al. 1991; Martin et al. 2011). This systematic difference could result in cyclic transitions between the low- \dot{m} and the high- \dot{m} states. Another possibility is that the orbital period jumps are stochastic — an atypically large negative jump can trigger a temporary bootstrapping phase.

4.2.3 Hydrogen burning stability

The high self-sustaining accretion rates that we find $\dot{m} \sim 10^{-7} \text{ M}_{\odot} \text{ yr}^{-1}$ are close to the hydrogen burning stability limit (Nomoto et al. 2007; Shen & Bildsten 2007; Wolf et al. 2013). If \dot{m} is high enough, then depending on its mass, a white dwarf may stably burn accreted hydrogen instead of erupting as recurrent novae. In Fig. 5 we repeat the calculation of the self-sustaining \dot{m} for a range of white dwarf masses M and compare it to the stability limit. Fig. 5 indicates that massive white dwarfs with low-mass companions tend to erupt as (recurrent) novae during bootstrapping, whereas lighter white dwarfs with massive companions burn hydrogen stably. White dwarfs in CVs are typically massive in comparison to their solitary counterparts, with an average $M \approx 0.8 \text{ M}_{\odot}$ (Knigge 2006; Savoury et al. 2011; Zorotovic et al. 2011). For such a typical white dwarf, the critical companion mass above which burning is stable is $m \approx 0.2 \text{ M}_{\odot}$, coincidentally close to the mass at the famous CV orbital period gap ($\approx 2 - 3 \text{ h}$, see Knigge et al. 2011). We conclude that short-period CVs (below the gap) like T Pyx (1.8 h) and IM Nor (2.5 h) tend to erupt as recurrent novae when the mass transfer is self-sustaining, whereas long-period CVs (above the gap) can burn hydrogen stably.

Stable nuclear burning increases the white dwarf’s luminosity by a factor of $f \approx 30$ compared to gravitational energy release for the same \dot{m} (e.g. Wolf et al. 2013), leading to stronger irradiation $T_{\text{irr}}^4 \propto \dot{m} f$. Using our analytical scaling $\dot{m} \propto T_{\text{irr}}^{5/3}$, the self-sustaining mass transfer rate is higher by a factor of $\dot{m} \propto f^{5/7} \approx 10$. This suggests a self-sustaining $\dot{m} \sim 10^{-6} \text{ M}_{\odot} \text{ yr}^{-1}$, which is sufficiently high such that the white dwarf cannot steadily burn all of the accreted hydrogen (i.e. above the top dashed green line in Fig. 5; see Wolf et al. 2013). We speculate that the burning rate saturates at the maximal stable value, and the rest of \dot{m} is blown away in a wind (Hachisu et al. 1996).

Stable burning at rates of $\sim 10^{-7} \text{ M}_{\odot} \text{ yr}^{-1}$ appears as a prolonged supersoft X-ray phase (Kahabka & van den Heuvel 1997). Supersoft sources are usually explained by either post-nova burning of a residual hydrogen envelope that is exhausted within several years (for a 0.8 M_{\odot} white dwarf, see Soraisam et al. 2016), or by unstable mass transfer on a thermal time-scale from a massive donor ($m \gtrsim 1.3 \text{ M}_{\odot}$ and also heavier than the white dwarf, see van den Heuvel et al. 1992; Kahabka & van den Heuvel 1997). Some sources, however, fit neither of these scenarios: the orbital periods of RX J0537.7–7034 (3.5 h) and 1E 0035.4–7230 (4.1 h) are too short for a massive companion, and yet their supersoft emission persists for many decades (van Teeseling & King 1998; Greiner et al. 2000; King et al. 2001). These sources, with periods above the gap, are naturally explained by our model as the result of self-sustaining mass transfer induced by irradiation. van Teeseling & King (1998) proposed a similar idea, but in their case an irradiation-driven wind pushes the companion towards Roche-lobe overflow by carrying away angular momentum

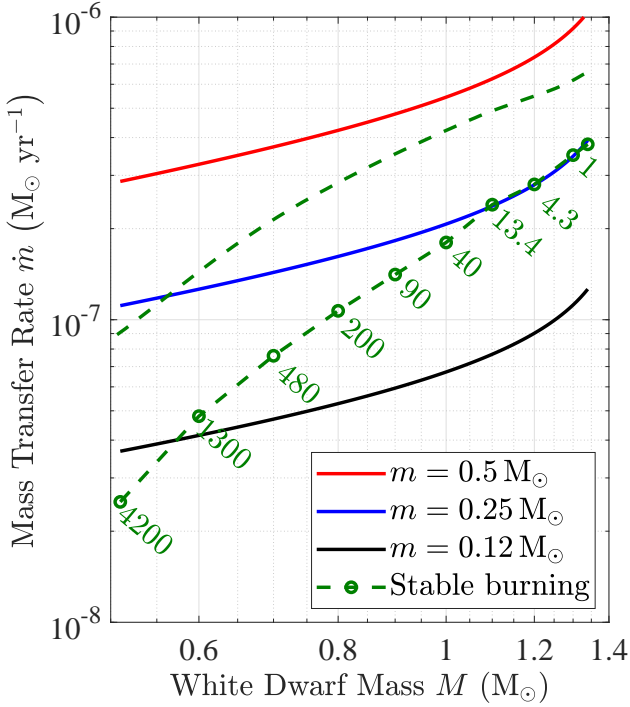


Figure 5. Self-sustaining mass transfer rates \dot{m} (assuming $\Delta r_L = 0$) as a function of the white dwarf’s mass M for different companion masses m . The rates are calculated by equating $\dot{m} \propto m^{1.3} T_{\text{irr}}^{5/3}$ (calibrated using Fig. 3) to $\dot{m} = 16\pi a^2 \sigma T_{\text{irr}}^4 R / (GM)$; we take $R(M)$ from Hansen et al. (2004) and calculate $a(M, m)$ using Eggleton (1983). Below the bottom dashed green line (given by Wolf et al. 2013), \dot{m} drives recurrent nova eruptions. Above the line, the white dwarf burns accreted hydrogen stably, powering a supersoft X-ray source. During stable burning, nuclear power increases the irradiation and hence \dot{m} . We assume that the mass burning rate saturates at its maximal stable value (the top dashed green line, given by Wolf et al. 2013), and that the rest of \dot{m} is blown away in a wind, as suggested by Hachisu et al. (1996). The nova recurrence times just below stability are labelled in years (from Wolf et al. 2013).

— our inflation mechanism applies even when mass and angular momentum are conserved (see also Knigge et al. 2000, who applied the van Teeseling & King 1998 mechanism to T Pyx). Shen et al. (2009) found that helium core white dwarfs (with $M < 0.5 M_\odot$) enter prolonged supersoft phases after novae, potentially explaining RX J0537.7–7034 and 1E 0035.4–7230. Our scenario, on the other hand, is also valid for regular CVs with typical-mass white dwarfs. In our case, the rareness of such systems may be attributed to the requirement of a small Roche-lobe offset Δr_L , similarly to T Pyx and IM Nor (Section 4.2.1).

5 SUMMARY

The donor stars in CVs are irradiated during novae by luminosities that exceed their own by several orders of magnitude. We revisited the response of the donor to this irradiation, focusing on the mass transfer \dot{m} that is induced by the donor’s inflation beyond its Roche lobe. We calculated the penetration of heat into the donor’s atmosphere both analytically and using MESA. We coupled the heating to the mass transfer and derived $\dot{m} \propto m^{1.3} T_{\text{irr}}^{5/3}$, where m is the donor’s mass, and T_{irr} is the irradiation temperature on its surface. Our calculation improves upon previous studies (Kovetz et al. 1988;

Hillman et al. 2020) by consistently computing the mass and density of the heated zone that overflows the Roche lobe, rather than assuming a constant photospheric density. We find mass transfer rates that are more than an order of magnitude higher than previously thought — $\dot{m} \sim 10^{-6} M_\odot \text{ yr}^{-1}$ at the peak of the nova eruption.

As the nova subsides and T_{irr} declines, \dot{m} drops to lower values. However, we identified a self-sustaining state in which the white dwarf’s accretion luminosity itself is sufficient to drive mass transfer by irradiation at a rate of $\dot{m} \sim 10^{-7} M_\odot \text{ yr}^{-1}$ long after the eruption. This ‘bootstrapping’ state is manifested differently depending on the CV’s orbital period (which is linked to the donor’s mass through the Roche-lobe filling condition). For a typical CV white dwarf with $M \approx 0.8 M_\odot$ (Zorotovic et al. 2011), the critical period that determines the nature of the self-sustaining state coincides with the famous $\approx 2 - 3$ h period gap (Knigge et al. 2011):

(i) Short-period CVs erupt as recurrent novae. Bootstrapping may explain the high accretion rates measured for the recurrent novae T Pyx and IM Nor between eruptions, as well as their short recurrence times (Patterson et al. 2017, 2020; Godon et al. 2018).

(ii) Long-period CVs burn hydrogen stably and appear as supersoft X-ray sources. Bootstrapping may explain the prolonged (longer than the several years that are expected post nova, see Soraisam et al. 2016) supersoft emission from RX J0537.7–7034 and 1E 0035.4–7230. With orbital periods of 3.5 and 4.1 h, these objects defy the standard explanation which invokes mass transfer on a thermal time-scale from especially massive donors (King et al. 2001).

Over the course of $\sim 10^3$ yr, stable mass transfer at this high rate increases the donor’s Roche lobe, lowering \dot{m} and T_{irr} , until the star no longer overflows its Roche lobe — bootstrapping ceases and \dot{m} plummets. We compared this time-scale to the rate at which gravitational waves and magnetic braking tend to shrink the Roche lobe and estimated that only about 10^{-3} of CVs are currently in the bootstrapping state. Nonetheless, novae recur $\sim 10^3$ times more often during bootstrapping (thanks to the higher accretion rate, see Chomiuk et al. 2020), such that a significant fraction of nova eruptions may evolve to this state as the white dwarf cools — broadly consistent with the occurrence of T Pyx and IM Nor.

We conclude that novae trigger episodes of fast mass transfer by irradiation: $\dot{m} \sim 10^{-6} M_\odot \text{ yr}^{-1}$ at the peak of the eruption and, under certain circumstances (Section 4.2.1), a self-sustaining $\dot{m} \sim 10^{-7} M_\odot \text{ yr}^{-1}$ that persists long after the eruption subsides. The occurrence rate and duration of the self-sustaining phase depend critically on how the donor’s Roche lobe evolves over time and through multiple nova cycles. If all donor stars and all novae were identical, all systems at a given orbital period and with a given white dwarf mass would evolve the same way after a nova: either into a self-sustaining state or not, depending on the Roche lobe’s size during quiescence and during an eruption. This is inconsistent with the fact that systems at the same orbital period appear to have quite different accretion rates years after novae. We speculate that this difference is due to variation in either the surface layer structure of the donor or the mass and angular momentum lost during novae, both of which are critical for determining if the self-sustaining state is realized. Because of these uncertainties, we cannot robustly test our predictions using the fraction of systems that appear to be in the self-sustaining state. Nevertheless, the bootstrapping mechanism naturally provides a unified explanation for two puzzling classes of close binaries: long-lived supersoft sources with short orbital periods, and recurrent novae with even shorter periods.

ACKNOWLEDGEMENTS

We thank Yael Hillman, Brian Metzger, and Ken Shen for comments and for illuminating discussions. SG is supported by the Heising-Simons Foundation through a 51 Pegasi b Fellowship. This work benefited from workshops supported by the Gordon and Betty Moore Foundation through Grant GBMF5076

DATA AVAILABILITY

The data underlying this article will be shared on reasonable request to the corresponding author.

REFERENCES

- Avrett E. H., Loeser R., 2008, *ApJS*, **175**, 229
- Chomiuk L., Metzger B. D., Shen K. J., 2020, arXiv e-prints, [p. arXiv:2011.08751](https://arxiv.org/abs/2011.08751)
- Eggleton P. P., 1983, *ApJ*, **268**, 368
- Gallagher J. S., Starrfield S., 1978, *ARA&A*, **16**, 171
- Gehrz R. D., Truran J. W., Williams R. E., Starrfield S., 1998, *PASP*, **110**, 3
- Godon P., Sion E. M., Williams R. E., Starrfield S., 2018, *ApJ*, **862**, 89
- Greiner J., Orio M., Schwarz R., 2000, *A&A*, **355**, 1041
- Hachisu I., Kato M., Nomoto K., 1996, *ApJ*, **470**, L97
- Hansen C. J., Kawaler S. D., Trimble V., 2004, *Stellar interiors : physical principles, structure, and evolution*. Springer
- Harpaz A., Rappaport S., 1991, *ApJ*, **383**, 739
- Hillman Y., Prialnik D., Kovetz A., Shara M. M., Neill J. D., 2014, *MNRAS*, **437**, 1962
- Hillman Y., Shara M. M., Prialnik D., Kovetz A., 2020, *Nature Astronomy*, **4**, 886
- Kahabka P., van den Heuvel E. P. J., 1997, *ARA&A*, **35**, 69
- King A. R., Schenker K., Kolb U., Davies M. B., 2001, *MNRAS*, **321**, 327
- Kippenhahn R., Weigert A., Weiss A., 2012, *Stellar Structure and Evolution*. Springer, [doi:10.1007/978-3-642-30304-3](https://doi.org/10.1007/978-3-642-30304-3)
- Knigge C., 2006, *MNRAS*, **373**, 484
- Knigge C., King A. R., Patterson J., 2000, *A&A*, **364**, L75
- Knigge C., Baraffe I., Patterson J., 2011, *ApJS*, **194**, 28
- Kolb U., Ritter H., 1990, *A&A*, **236**, 385
- Kovetz A., Prialnik D., Shara M. M., 1988, *ApJ*, **325**, 828
- Linial I., Sari R., 2017, *MNRAS*, **469**, 2441
- Livio M., Govarie A., Ritter H., 1991, *A&A*, **246**, 84
- Lubow S. H., Shu F. H., 1975, *ApJ*, **198**, 383
- Marsh T. R., Nelemans G., Steeghs D., 2004, *MNRAS*, **350**, 113
- Martin R. G., Livio M., Schaefer B. E., 2011, *MNRAS*, **415**, 1907
- Nomoto K., Saio H., Kato M., Hachisu I., 2007, *ApJ*, **663**, 1269
- Paczynski B., Sienkiewicz R., 1972, *Acta Astron.*, **22**, 73
- Patterson J., 1984, *ApJS*, **54**, 443
- Patterson J., et al., 2017, *MNRAS*, **466**, 581
- Patterson J., et al., 2020, arXiv e-prints, [p. arXiv:2010.07812](https://arxiv.org/abs/2010.07812)
- Paxton B., Bildsten L., Dotter A., Herwig F., Lesaffre P., Timmes F., 2011, *ApJS*, **192**, 3
- Paxton B., et al., 2013, *ApJS*, **208**, 4
- Paxton B., et al., 2015, *ApJS*, **220**, 15
- Paxton B., et al., 2018, *ApJS*, **234**, 34
- Paxton B., et al., 2019, *ApJS*, **243**, 10
- Prialnik D., 1986, *ApJ*, **310**, 222
- Prialnik D., Kovetz A., 1995, *ApJ*, **445**, 789
- Rappaport S., Joss P. C., Webbink R. F., 1982, *ApJ*, **254**, 616
- Rappaport S., Verbunt F., Joss P. C., 1983, *ApJ*, **275**, 713
- Ritter H., 1988, *A&A*, **202**, 93
- Salazar I. V., LeBleu A., Schaefer B. E., Landolt A. U., Dvorak S., 2017, *MNRAS*, **469**, 4116
- Savonije G. J., 1978, *A&A*, **62**, 317
- Savourey C. D. J., et al., 2011, *MNRAS*, **415**, 2025
- Schaefer B. E., 2020, *MNRAS*, **492**, 3343
- Schreiber M. R., Zorotovic M., Wijnen T. P. G., 2016, *MNRAS*, **455**, L16
- Shara M. M., 1989, *PASP*, **101**, 5
- Shara M. M., Livio M., Moffat A. F. J., Orio M., 1986, *ApJ*, **311**, 163
- Shen K. J., Bildsten L., 2007, *ApJ*, **660**, 1444
- Shen K. J., Idan I., Bildsten L., 2009, *ApJ*, **705**, 693
- Soraisam M. D., Gilfanov M., Wolf W. M., Bildsten L., 2016, *MNRAS*, **455**, 668
- Spruit H. C., Ritter H., 1983, *A&A*, **124**, 267
- Townsley D. M., Bildsten L., 2004, *ApJ*, **600**, 390
- Wolf W. M., Bildsten L., Brooks J., Paxton B., 2013, *ApJ*, **777**, 136
- Yaron O., Prialnik D., Shara M. M., Kovetz A., 2005, *ApJ*, **623**, 398
- Zorotovic M., Schreiber M. R., Gänsicke B. T., 2011, *A&A*, **536**, A42
- van Teeseling A., King A. R., 1998, *A&A*, **338**, 957
- van den Heuvel E. P. J., Bhattacharya D., Nomoto K., Rappaport S. A., 1992, *A&A*, **262**, 97

This paper has been typeset from a $\mathrm{T}_{\mathrm{E}}\mathrm{X}/\mathrm{L}^{\mathrm{A}}\mathrm{T}_{\mathrm{E}}\mathrm{X}$ file prepared by the author.